Epitaxial Growth of a Single-Domain Hexagonal Boron Nitride Monolayer

Fabrizio Orlando,[†,#] Paolo Lacovig,[‡] Luca Omiciuolo,[†] Nicoleta G. Apostol,[‡,§] Rosanna Larciprete,[⊥] Alessandro Baraldi,[†,‡,∥] and Silvano Lizzit*[,‡]

[†]Physics Department, University of Trieste, Via Valerio 2, 34127 Trieste, Italy, [‡]Elettra-Sincrotrone Trieste S.C.p.A., AREA Science Park, S.S. 14 km 163.5, 34149 Trieste, Italy, [§]National Institute of Materials Physics, Atomistilor 105b, 077125 Magurele-Ilfov, Romania, [⊥]CNR-Institute for Complex Systems, Via Fosso del Cavaliere 100, 00133 Roma, Italy, and [∥]IOM-CNR, Laboratorio TASC, AREA Science Park, S.S. 14 km 163.5, 34149 Trieste, Italy. [#]Present address: Laboratory of Radiochemistry and Environmental Chemistry, Paul Scherrer Institute, 5232 Villigen, Switzerland.

ABSTRACT We investigate the structure of epitaxially grown hexagonal boron nitride (*h*-BN) on Ir(111) by chemical vapor deposition of borazine. Using photoelectron diffraction spectroscopy, we unambiguously show that a single-domain *h*-BN monolayer can be synthesized by a cyclic dose of high-purity borazine onto the metal substrate at room temperature followed by annealing at $T = 1270$ K, this method giving rise to a diffraction pattern with 3-fold symmetry. In contrast, high-temperature borazine deposition ($T = 1070$ K) results in a *h*-BN monolayer formed by domains with opposite orientation and characterized by a 6-fold symmetric diffraction pattern. We identify the thermal energy and the binding energy difference between fcc and hcp seeds as key parameters in controlling the alignment of the growing *h*-BN clusters during the first stage of the growth, and we further propose structural models for the *h*-BN monolayer on the Ir(111) surface.

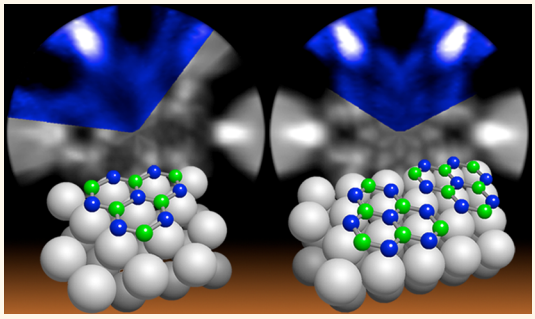

KEYWORDS: hexagonal boron nitride · Ir(111) · chemical vapor deposition · temperature-programmed growth · X-ray photoelectron diffraction

Two-dimensional (2D) atomic crystals[1] have received a great deal of attention in the last years, owing to their distinct properties that could be exploited in a variety of applications, including electronics, optoelectronics, spintronics, chemical sensors, catalysis, energy storage, *etc*.[2] Within the family of 2D layered materials, hexagonal boron nitride (*h*-BN),[3,4] a single sheet of alternating boron and nitrogen atoms arranged in a sp^2-honeycomb lattice, occupies a special position, being an insulator[5] isostructural to graphene.[6,7] The use of *h*-BN as a dielectric substrate for graphene transistors has been shown to significantly improve the carrier mobility in graphene.[8] Moreover, the possibility of combining *h*-BN and graphene to build up more complex heterostructures,[9] shows promise for replacing silicon in future electronics.[10]

The potential application of *h*-BN in electronic devices demands scalable methods for producing large-area high-quality layers. Chemical vapor deposition (CVD) has been successfully employed to synthesize single *h*-BN layers on a number of different metal substrates by using borazine ($B_3N_3H_6$) as a precursor.[11−15] A strategy to improve the quality of the *h*-BN film is to apply low precursor pressure combined with high substrate temperature,[16] or to simultaneously expose the metal surface to borazine and hydrogen.[17] Nevertheless, it is challenging to obtain large single crystalline domains because of the formation of rotated phases that give rise to grain boundaries and other 1D defects.[18] For instance, the nucleation of rotational domains has been reported for systems characterized by a weak interfacial bonding, like Pd(111),[19] Cu(111),[20] and Ag(111).[21] Moreover, the formation of misoriented domains has been observed also in the case of substrates with strongly chemisorbed *h*-BN monolayers, such as Ni(111)[22] and Rh(111).[16] The origin of the rotational domains has been traced back to factors like commensurability, symmetry, interaction with the substrate, and also chemistry of the precursor.[19,23,24] To date, however, the relative abundance of these structures is far from being controlled. Hence, much effort is still needed in order to achieve the highest quality for *h*-BN films on metal surfaces.

* Address correspondence to silvano.lizzit@elettra.eu.

Received for review October 18, 2013 and accepted November 12, 2014.

Published online November 12, 2014
10.1021/nn5058968

© 2014 American Chemical Society

Here we demonstrate a CVD method for producing a *h*-BN monolayer with single orientation on Ir(111) by properly controlling the growth conditions. We adopted two different strategies to grow *h*-BN using borazine as a precursor and subsequently characterized the resulting layers by means of X-ray photoelectron spectroscopy (XPS), X-ray photoelectron diffraction (XPD), and low energy electron diffraction (LEED). We find that, while the ordinary high-temperature borazine deposition gives rise to a *h*-BN monolayer formed by domains with opposite orientation, a *h*-BN monolayer with single orientation can be synthesized by dosing borazine at room temperature and subsequently annealing the sample. Spot profile analysis (SPA)-LEED measurements show that the average domain size is larger than 900 Å. Our results provide new insight into the strategies for producing *h*-BN monolayers with single orientation.

RESULTS AND DISCUSSION

Two different procedures have been followed to grow *h*-BN on Ir(111). The first method consisted of exposing the Ir surface at $T = 1070$ K to $p = 5 \times 10^{-8}$ mbar of borazine, up to a total exposure of about 10^2 L (1 L = 1 Torr·s) (high temperature growth (HTG)).[25] The second approach, instead, consisted of repeated cycles of borazine dosing at room temperature at $p \approx 1 \times 10^{-8}$ mbar until saturation of the surface, followed by annealing to $T = 1270$ K, with 4 K s^{-1} heating rate (temperature-programmed growth (TPG)). The TPG method is commonly used to grow high-quality graphene single-layers on Ir(111) by ethylene exposure.[26] Both approaches ensure the growth of an extended single-layer *h*-BN that does not leave bare Ir regions (see Supporting Information). The completeness of the *h*-BN layer was proved by measuring the B 1s, N 1s, and Ir $4f_{7/2}$ spectra, which did not change over the sample surface or by prolonging the growth time. It is noteworthy that this method detects variations of the B and N coverages as low as 1%.

Figure 1a,b shows the LEED patterns from the *h*-BN layers synthesized as described above. The images prove the growth of the *h*-BN layers for both approaches (see also zoom-in in the insets). Indeed, the observed patterns are in line with the previously reported 13 × 13/12 × 12 superstructure:[14] the principal substrate spots are surrounded by sharp noninteger moiré satellites, indicating the formation of long-range ordered *h*-BN. The absence of additional diffraction features that are rotated with respect to the first-order iridium-induced spots indicates that, for both synthesis conditions, the *h*-BN unit cell is aligned parallel to the lattice of the substrate. However, a comparison of the LEED intensities reveals a major difference for the two growth procedures. While the iridium-induced spots always show the expected 3-fold symmetry, the pattern from the *h*-BN layer

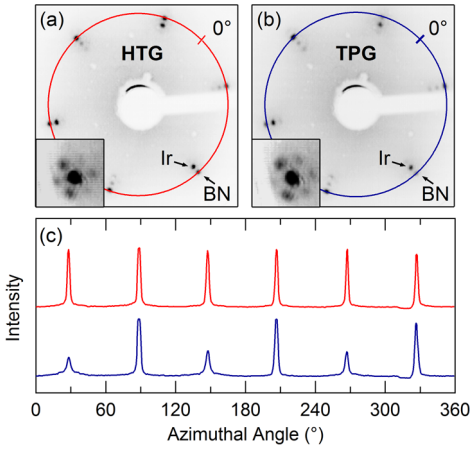

Figure 1. LEED patterns meaured at 83 eV for *h*-BN synthesized according to (a) HTG and (b) TPG procedures. Insets: zoom-in of the principal spots measured at 55 eV. (c) The 6- and 3-fold symmetry of the patterns is clearly shown by the line profile analysis along the colored rings containing the BN spots in (a) and (b), red and blue lines, respectively.

grown with the HTG method (Figure 1a) exhibits moiré-spots with 6-fold symmetry, as shown by the red intensity distribution plot in Figure 1c. On the other hand, for the TPG procedure, also the BN-related spots are 3-fold symmetric (blue curve in Figure 1c). Notably, this behavior has not been observed so far. Indeed, the LEED patterns reported in literature for lattice-mismatched *h*-BN/transition metal interfaces always show moiré intensities with 6-fold symmetry.[13,19,27,28] Only for the lattice-matched Cu surface has a 3-fold symmetric pattern been measured, but in this case it is not possible to disentangle the contributions from the substrate and the *h*-BN layer because of the overlap of the corresponding LEED spots.[29]

To gain further insight into the structural properties of the *h*-BN/Ir(111) interface, XPS and XPD techniques were employed to characterize the chemical composition and structure of the system. Figure 2a and Figure 2b show the B 1s and N 1s core level spectra for the *h*-BN layer prepared according to the HTG procedure. No significant differences were found in the photoemission spectra for the two preparations. As already pointed out in previous works,[14,25,30] the two-components structure in the B 1s and N 1s core levels reflects different strengths of the BN−Ir interaction: a main peak due to *h*-BN regions weakly interacting with the iridium surface (B_0 and N_0), and a minor contribution from *h*-BN regions strongly interacting with the substrate (B_1 and N_1).

The lower part of Figure 2 depicts selected B 1s and N 1s XPD patterns for the two preparations (colored sectors), together with their multiple scattering simulations (gray regions), for two different photon energies, corresponding to photoelectron kinetic energies (E_k) of 115 and 315 eV. The simulations have been performed with the program package for Electron Diffraction in Atomic Cluster (EDAC)[31]

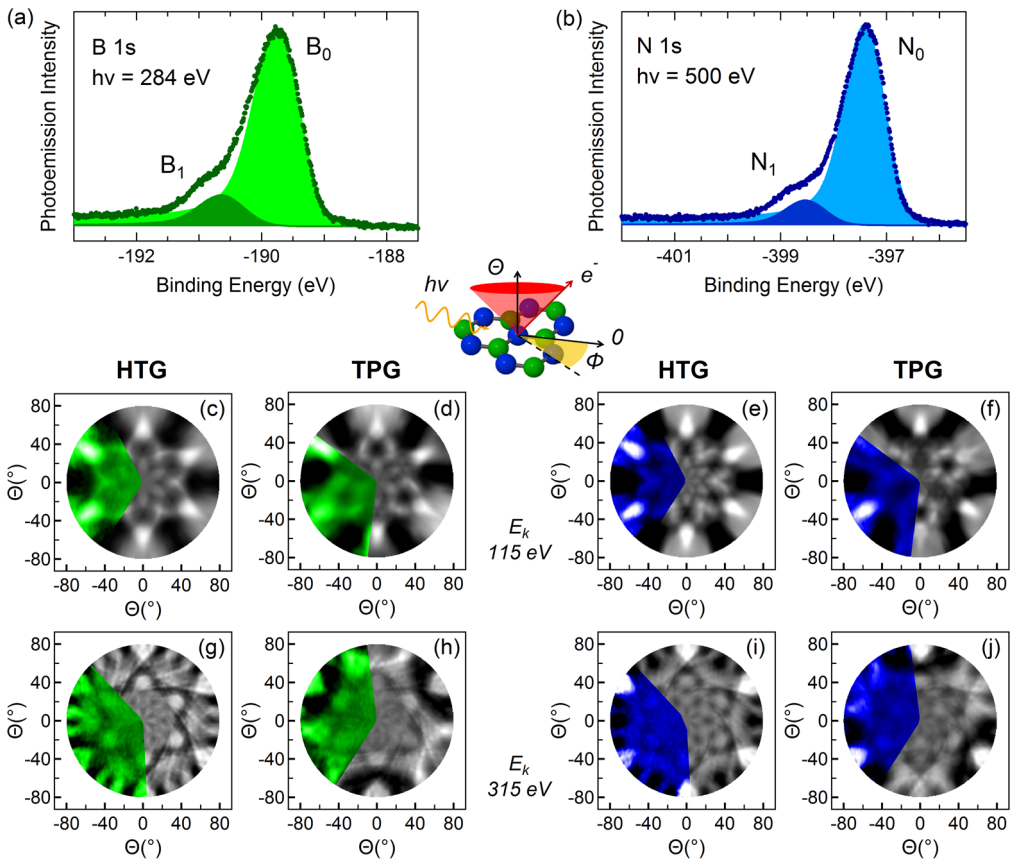

Figure 2. B 1s (a) and N 1s (b) core level spectra together with the spectral contributions resulting from peak-fit analysis. (c−j) Stereographic projection of the integrated photoemission intensity modulation $I(\theta, \phi)$ as a function of emission angle for B 1s (left) and N 1s (right) core level. The colored sector is the experimental data, while the gray region is the calculation for a flat, free-standing *h*-BN layer.

for a free-standing, flat *h*-BN layer. No symmetry was imposed to the experimental data.

Let us consider the XPD patterns corresponding to the HTG preparation. Both B 1s and N 1s data exhibit similar diffraction features, with intensity maxima that are clearly visible close to grazing emission angles (Figure 2c,e,g,i). These patterns are 6-fold symmetric, consistently with the presence of two antiparallel *h*-BN domains. To better understand this point, the geometry of the *h*-BN layer on the Ir substrate is depicted in Figure 3, showing the two possible orientations for a 13 × 13/12 × 12 superstructure keeping the same azimuthal alignment as that of the underlying (111) surface, in accordance with the LEED findings. The domains are rotated by 180° relative to each other. Indeed, the boron and nitrogen atoms positions are inverted in the corresponding unit cells. If both structures grow on the surface with the same probability and distribution, then we expect the resulting diffraction pattern to be 6-fold symmetric, as those obtained by the first growth procedure. In sharp contrast with these findings, the second preparation gives rise to 3-fold symmetric diffraction patterns (Figure 2d,f,h,j), indicating the prevalence of only one *h*-BN orientation. A close comparison of the B 1s and N 1s XPD patterns shows not only their 180° misorientation, related to the nonequivalent positions of boron and nitrogen atoms in the unit cell, but also appreciable differences in the diffraction features due to different scatterers in the same structural configuration (see also Figure 4a,b). These results clearly indicate that the synthesis conditions affect the orientation of the *h*-BN layer. Our interpretation is further supported by the very good agreement with the simulated photoemission intensities, which have been performed considering both *h*-BN domains depicted in Figure 3 (HTG), or just one of these (TPG).

So far, the emergence and coexistence of multiple *h*-BN domains has been reported on several metal surfaces. As previously mentioned, domains without preferential orientation develop on weakly interacting substrates such as Pd,[19] Cu,[20] and Ag.[21] For the strongly bonded *h*-BN/Rh(111) interface, instead, the symmetry of the domains is the same as that of the substrate, although 180° misoriented islands have been observed.[16] Previous experimental findings[30] and theoretical predictions[32] suggest that the chemical interaction of *h*-BN on Ir(111) is slightly weaker compared to that on Rh(111), where the monolayer is strongly chemisorbed. For the commensurate *h*-BN/Ni(111)

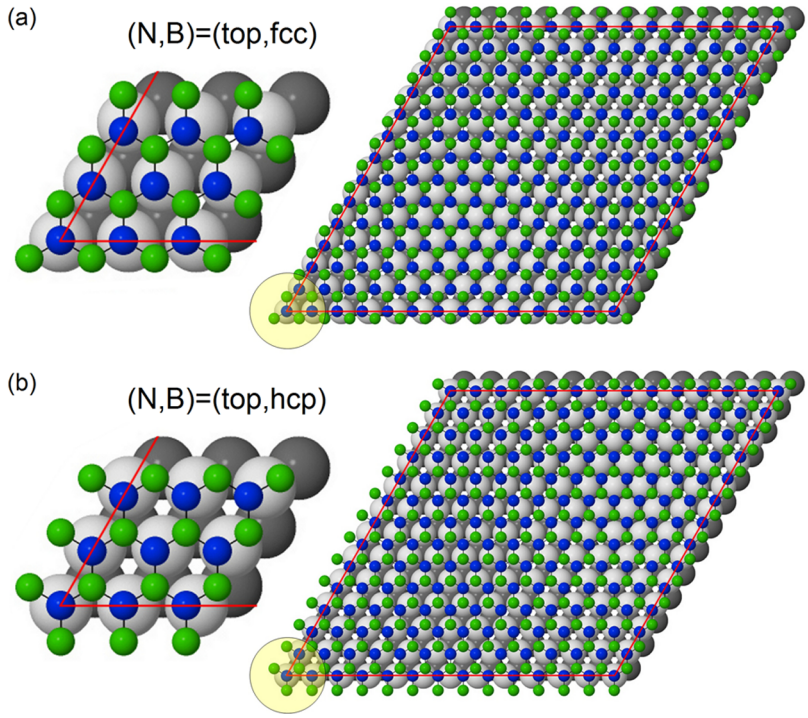

Figure 3. Possible 13 × 13/12 × 12 *h*-BN/Ir(111) configurations. The insets on the left show the adsorption configuration of the bonding regions (see text for details).

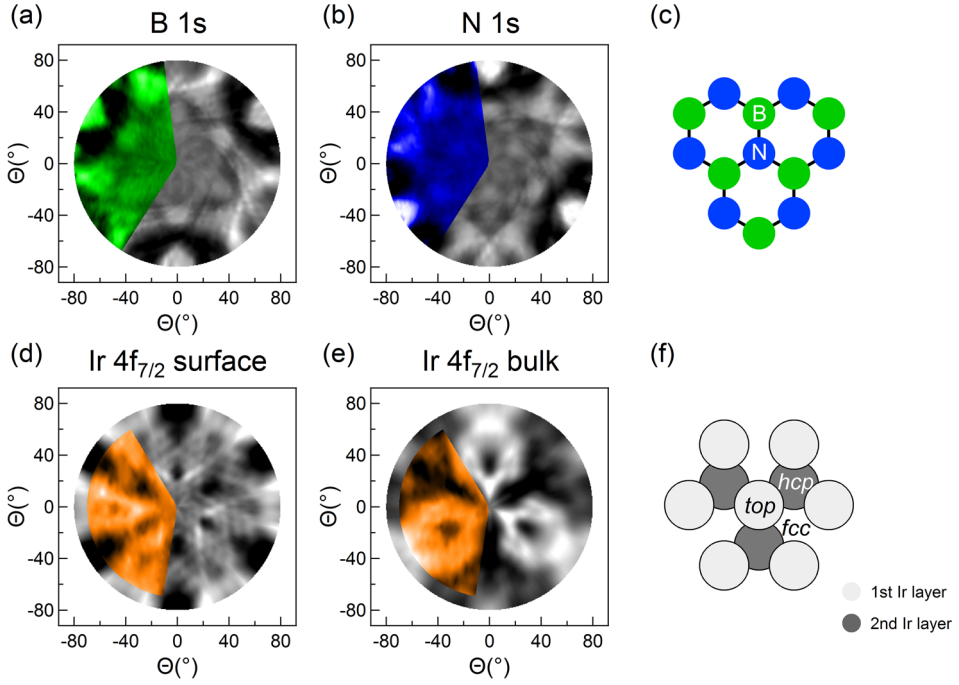

Figure 4. XPD patterns for B 1s (a) and N 1s (b) core levels (E_k = 315 eV), and Ir $4f_{7/2}$ from surface (d) and bulk (e) atoms (E_k = 120 eV). The geometric structures used to simulate these patterns are shown in (c) and (f) for the *h*-BN layer and the Ir(111) substrate, respectively. The simulations of the Ir patterns have been performed for the clean surface.

interface, the formation of two antiparallel domains has been reported, corresponding to a unit cell with N on top of nickel and B on fcc (N_{top},B_{fcc}) or hcp (N_{top},B_{hcp}) sites.[22,33] It has been suggested that small amounts of carbon contamination may control the ratio between these domains.[22]

The absence of carbon or other impurities was carefully checked by XPS (detection limit of 1% of a monolayer), thus we can safely rule out the possibility proposed in ref 22. What is therefore the factor that sets limits on the formation of both domains for the TPG growth? A plausible scenario is that nuclei with a

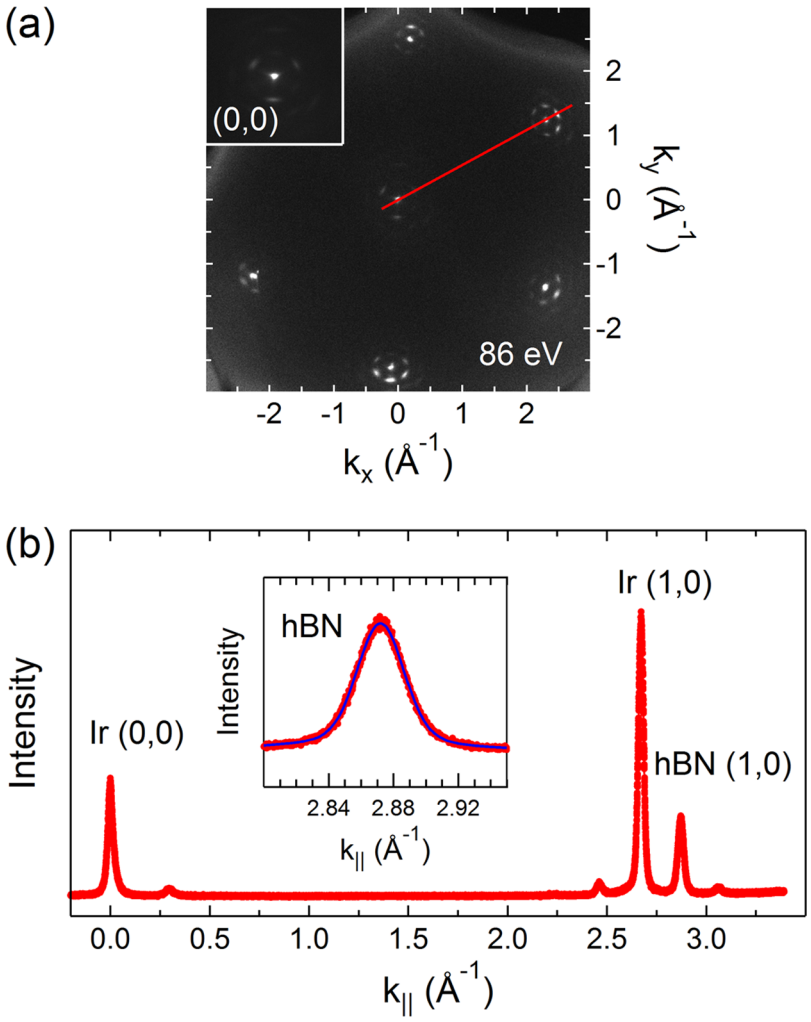

Figure 5. (a) SPA-LEED image of the singly oriented *h*-BN monolayer measured at kinetic energy of 86 eV, together with a zoom of the zero-order diffraction spot. (b) Spot profile analysis along the [10] direction. The inset displays the best fit analysis of the (1,0) *h*-BN diffraction spot.

well-defined alignment are already established at the first stages of the growth, and that these seeds expand while keeping their initial orientation. Theoretical calculations show that for the commensurate *h*-BN/Ni(111) interface the bonding configurations are (N_{top},B_{hcp}) and (N_{top},B_{fcc}), the latter being energetically favored.[34] The situation is only slightly different for lattice-mismatched interfaces, where periodic repetitions of different coordination sites give rise to a moiré pattern. Nonetheless, the (N_{top},B_{fcc}) configuration is predicted to be stable also for these systems, meaning that the regions where the *h*-BN sheet is closer to the substrate develop around this configuration.[35,36] Theoretical calculations based on local-density approximation, where a 1 × 1 commensurate geometry has been applied, predict a weaker strength of the binding energy of *h*-BN on Ni compared to that on Ru(0001) whose bonding, instead, is comparable to that of Rh(111) and Ir (111).[32] Moreover, the difference between the binding energy of *h*-BN/Ni(111) and *h*-BN/Ru(0001) is even larger when taking into account the lattice mismatch of the latter interface.[37] Accordingly, it is plausible to assume the (N_{top},B_{fcc}) to be a bonding configuration also for the initial stages of *h*-BN growth on the Ir(111) surface.

On the basis of these considerations, we thus propose the following mechanism for *h*-BN growth on Ir with the TPG approach. When the surface is exposed to borazine at room temperature and then annealed, the nucleation starts in the lowest energy configuration: the small BN islands adopt a single orientation relative to the substrate, which very likely corresponds to a fcc domain. Notably, in a previous work on the *h*-BN/Ir(111) interface,[14] we already pointed out that borazine dehydrogenation is observed above 250 K. This could therefore indicate that boron and nitrogen atoms are potentially able to couple and interact with the Ir surface atoms already at room temperature. As the growth proceeds, the fcc nucleation seeds expand forming larger BN clusters which keep the initial orientation. This can be explained as due to the energy difference between the fcc and hcp configurations, in analogy to the growth of *h*-BN on Ru(0001).[37] Indeed,

in this case the adsorption energy difference per B atom of the BN clusters with increasing number of rings keeps constant, with the fcc clusters being more stable. Therefore, as the width of the BN nucleation seeds increases, the energy difference between fcc and hcp gets higher, thus allowing the growth of a single domain with the same fcc configuration of the initial seeds. For the synthesis performed directly at high temperature, on the other hand, the thermal energy is sufficient to exceed the energy difference between the fcc and hcp adsorption configuration of the BN seeds during the initial stages of the CVD process. As a result, both nucleation seeds form, and two antiparallel *h*-BN domains develop. Interestingly, the STM measurements on the *h*-BN/Ru(0001) nanomesh[37] show a parallel alignment of growing fcc islands within the same Ru terrace when the growth is performed at 700 K, while hcp domains appear when borazine is dosed at temperatures higher than 950 K.

We compared the experimental XPD patterns with simulations corresponding to different percentages of the fcc domain and computed the respective *R*-factors. We applied this quantitative analysis to the diffraction patterns obtained with HTG and TPG procedures and found out that the fcc percentage is 50% and 100%, respectively, with an uncertainty of about 5% in both cases.

To provide a compelling evidence that the single domain structure obtained by the second preparation has a fcc orientation, we extended the XPD measurements to the Ir $4f_{7/2}$ core level. Indeed, by exploiting the 3-fold symmetry of the substrate and by comparison with the simulated intensities, these data allow a determination of the *h*-BN layer orientation with respect to the Ir(111) surface. The measured Ir $4f_{7/2}$ spectrum of clean Ir(111) (not shown here) displays the characteristic two components assigned to surface and bulk atoms.[38] Figure 4 shows the diffraction patterns for the B 1s (a) and N 1s (b) core levels (same patterns displayed in Figure 2h,j), and for the Ir $4f_{7/2}$ core level from the surface (d) and bulk (e) atoms measured on the clean substrate, that is, before the growth of the *h*-BN monolayer. The azimuthal orientation of the simulations is aligned to the geometric structure shown in Figure 4c and f for *h*-BN and Ir(111) lattices, respectively. Accordingly, this finding proves that the arrangement of the *h*-BN layer corresponds to the *fcc* configuration shown in Figure 3a.

To measure the average domain size of the singly oriented *h*-BN layer, we performed SPA-LEED high resolution k-space measurements of the diffraction spots. Figure 5a shows the two-dimensional SPA-LEED pattern at a kinetic energy of 86 eV, while the spot profile along the [10] direction is presented in Figure 5b. The inset in Figure 5b shows a detail on the (1,0) h-BN spot together with the best fit analysis obtained using a Voigt function. The Gaussian width is 0.03 $Å^{-1}$, while the Lorentzian full width at half-maximum (fwhm) is below 0.008 $Å^{-1}$, corresponding to an average fcc domain size larger than 900 Å, which is comparable to the expected width of the Ir terraces.

CONCLUSIONS

Our results prove that an extended *h*-BN monolayer with a single orientation can be grown on Ir(111) by using proper synthesis conditions. Two different preparations have been employed to grow *h*-BN from borazine precursor: (i) dose at 1070 K and (ii) cyclic depositions at room temperature followed by annealing at 1270 K. While the symmetry of the resulting layers is always the same as that of the Ir(111) substrate, 180° misoriented *h*-BN domains are formed by the first method, corresponding to fcc and hcp configurations. The second preparation, instead, gives rise only to the fcc phase. This behavior is related to a different interplay between the thermal energy and the binding energy difference between fcc and hcp seeds during the first stages of *h*-BN growth. This approach could be further exploited on other transition metal surfaces in order to control the orientation of the resulting *h*-BN films.

METHODS

The experiments (excluding the SPA-LEED measurements, see below) were performed at the SuperESCA beamline of the Elettra synchrotron radiation facility in Trieste (Italy). The experimental chamber is equipped with a Phoibos hemispherical electron energy analyzer (150 mm mean radius), implemented with a delay line detector developed in-house. The base pressure in the ultrahigh vacuum chamber is better than $p = 1 \times 10^{-10}$ mbar.

The Ir substrate was prepared by repeated cycles of Ar^+ sputtering, oxygen treatment between 600 and 1000 K, and flash annealing to 1470 K. The sample quality was checked with XPS from C 1s and Ir $4f_{7/2}$, and the surface order was verified by means of LEED, which exhibited a sharp and low background 1×1 pattern. The *h*-BN layers were grown by thermal decomposition of borazine on the iridium surface. Borazine was synthesized following the procedure described by Wideman *et al.*,[39] and stored below 250 K at all times to avoid its degradation. Prior to every deposition, borazine was regularly purified by repeated freeze–thaw cycles.

The B 1s and N 1s core level spectra were measured using photon energies of 284 and 500 eV, respectively, with an overall energy resolution ranging from 40 to 100 meV. The surface normal, the incident beam direction, and the electron emission direction are all in the same horizontal plane, with the angle between the photon beam and the analyzer fixed at 70°. The core level spectra were decomposed using a Doniach-Šunjić line shape[40] convoluted with a Gaussian. The background was assumed to be linear. All the binding energies presented in this work are referenced to the Fermi level, measured in the same experimental conditions.

XPD measurements were performed with photon energies corresponding to electron kinetic energies of 115, 120, and 315 eV. At each of these energies 1140 spectra were measured, corresponding to different polar (θ) and azimuthal (ϕ) angles settings. Each XPD pattern was measured over a wide azimuthal

sector, ranging from 120° to 140°, from normal (θ = 0°) to grazing emission (θ = 80°). The reported modulation functions were obtained for each polar emission angle θ from the peak intensity $I(\theta, \phi)$ as $(I(\theta, \phi) - I_0(\theta))/I_0(\theta)$, where $I_0(\theta)$ is the average intensity for each azimuthal scan.

SPA-LEED was performed at the Surface Science Laboratory of Elettra Sincrotrone Trieste using a commercial Omicron SPA-LEED with a transfer width better than 1000 Å.[41] The instrument was used both to acquire high-quality two-dimensional reciprocal space maps at a fixed energy and to measure one-dimensional high-resolution profiles along specific reciprocal space directions. Reciprocal space lengths in the SPA-LEED scans are given in units of $Å^{-1}$ and were calibrated using the known lattice parameter of Ir(111).[14] Line profile diffraction spots for a corrugated surface can be modeled using a Voigt-type line shape.[42] The Gaussian contribution accounts for the instrumental broadening, that is, the finite coherence length of the primary electron beam, and for the corrugation of the *h*-BN layer over the Ir(111) surface,[27] in analogy with previous LEEM and μ-LEED measurements on graphene showing that an increased layer corrugation results in a broadening of the diffraction spots.[42] The Lorentzian component stems from fluctuations in the short-range order, and its width is proportional to the correlation length of the surface.

Conflict of Interest: The authors declare no competing financial interest.

Acknowledgment. The authors thank S. Fornarini, and R. Zanoni for precious support in the production of borazine and for stimulating discussions. This work was sponsored by Italian Ministery for Research (MIUR), under the program PRIN2010-2011 for the project 'GRAF. Frontiers in Graphene Research: understanding and controlling Advanced Functionalities'.

Supporting Information Available: Fast XPS analysis of the HTG and TPG growth methods of *h*-BN. This material is available free of charge *via* the Internet at http://pubs.acs.org.

REFERENCES AND NOTES

1. Novoselov, K. S.; Jiang, D.; Schedin, F.; Booth, T. J.; Khotkevich, V. V.; Morozov, S. V.; Geim, A. K. Two-Dimensional Atomic Crystals. *Proc. Natl. Acad. Sci. U.S.A.* **2005**, *102*, 10451–10453.
2. Xu, M.; Liang, T.; Shi, M.; Chen, H. Graphene-like Two-Dimensional Materials. *Chem. Rev.* **2013**, *113*, 3766–3798.
3. Corso, M.; Auwärter, W.; Muntwiler, M.; Tamai, A.; Greber, T.; Osterwalder, J. Boron Nitride Nanomesh. *Science* **2004**, *303*, 217–220.
4. Nagashima, A.; Tejima, N.; Gamou, Y.; Kawai, T.; Oshima, C. Electronic Structure of Monolayer Hexagonal Boron Nitride Physisorbed on Metal Surfaces. *Phys. Rev. Lett.* **1995**, *75*, 3918–3921.
5. Watanabe, K.; Taniguchi, T.; Kanda, H. Direct-Bandgap Properties and Evidence for Ultraviolet Lasing of Hexagonal Boron Nitride Single Crystal. *Nat. Mater.* **2004**, *3*, 404–409.
6. Novoselov, K. S.; Geim, A. K.; Morozov, S. V.; Jiang, D.; Zhang, Y.; Dubonos, S. V.; Grigorieva, I. V.; Firsov, A. A. Electric Field Effect in Atomically Thin Carbon Films. *Science* **2004**, *306*, 666–669.
7. Geim, A. K.; Novoselov, K. S. The Rise of Graphene. *Nat. Mater.* **2007**, *6*, 183–191.
8. Dean, C. R.; Young, A. F.; Meric, I.; Lee, C.; Wang, L.; Sorgenfrei, S.; Watanabe, K.; Taniguchi, T.; Kim, P.; Hone, J. Boron Nitride Substrates for High-Quality Graphene Electronics. *Nat. Nanotechnol.* **2010**, *5*, 722–726.
9. Geim, A. K.; Grigorieva, I. V. Van der Waals Heterostructures. *Nature* **2013**, *499*, 419–425.
10. Britnell, L.; Gorbachev, R. V.; Jalil, R.; Belle, B. D.; Schedin, F.; Mishchenko, A.; Georgiou, T.; Katsnelson, M. I.; Eaves, L.; Morozov, S. V.; *et al.* Field-Effect Tunneling Transistor Based on Vertical Graphene Heterostructures. *Science* **2012**, *335*, 947–950.
11. Auwärter, W.; Kreutz, T.; Greber, T.; Osterwalder, J. XPD and STM Investigation of Hexagonal Boron Nitride on Ni(111). *Surf. Sci.* **1999**, *429*, 229–236.
12. Ćavar, E.; Westerström, R.; Mikkelsen, A.; Lundgren, E.; Vinogradov, A. S.; Ng, M. L.; Preobrajenski, A. B.; Zakharov, A. A.; Mårtensson, N. A Single h-BN Layer on Pt(111). *Surf. Sci.* **2008**, *602*, 1722–1726.
13. Preobrajenski, A. B.; Vinogradov, A. S.; Ng, M. L.; Ćavar, E.; Westerström, R.; Mikkelsen, A.; Lundgren, E.; Mårtensson, N. Influence of Chemical Interaction at the Lattice-Mismatched h-BN/Rh(111) and h-BN/Pt(111) Interfaces on the Overlayer Morphology. *Phys. Rev. B* **2007**, *75*, 245412.
14. Orlando, F.; Larciprete, R.; Lacovig, P.; Boscarato, I.; Baraldi, A.; Lizzit, S. Epitaxial Growth of Hexagonal Boron Nitride on Ir(111). *J. Phys. Chem. C* **2012**, *116*, 157–164.
15. Goriachko, A.; He, Y.; Knapp, M.; Over, H.; Corso, M.; Brugger, T.; Berner, S.; Osterwalder, J.; Greber, T. Self-Assembly of a Hexagonal Boron Nitride Nanomesh on Ru(0001). *Langmuir* **2007**, *23*, 2928–2931.
16. Dong, G.; Fourré, E. B.; Tabak, F. C.; Frenken, J. W. M. How Boron Nitride Forms a Regular Nanomesh on Rh(111). *Phys. Rev. Lett.* **2010**, *104*, 096102.
17. Sutter, P.; Lahiri, J.; Albrecht, P.; Sutter, E. Chemical Vapor Deposition and Etching of High-Quality Monolayer Hexagonal Boron Nitride Films. *ACS Nano* **2011**, *5*, 7303–7309.
18. Gibb, A. L.; Alem, N.; Chen, J.-H.; Erickson, K. J.; Ciston, J.; Gautam, A.; Linck, M.; Zettl, A. Atomic Resolution Imaging of Grain Boundary Defects in Monolayer Chemical Vapor Deposition-Grown Hexagonal Boron Nitride. *J. Am. Chem. Soc.* **2013**, *135*, 6758–6761.
19. Morscher, M.; Corso, M.; Greber, T.; Osterwalder, J. Formation of Single Layer h-BN on Pd(111). *Surf. Sci.* **2006**, *600*, 3280–3284.
20. Joshi, S.; Ecija, D.; Koitz, R.; Iannuzzi, M.; Seitsonen, A. P.; Hutter, J.; Sachdev, H.; Vijayaraghavan, S.; Bischoff, F.; Seufert, K.; *et al.* Boron Nitride on Cu(111): An Electronically Corrugated Monolayer. *Nano Lett.* **2012**, *12*, 5821–5828.
21. Müller, F.; Hüfner, S.; Sachdev, H.; Laskowski, R.; Blaha, P.; Schwarz, K. Epitaxial Growth of Hexagonal Boron Nitride on Ag(111). *Phys. Rev. B* **2010**, *82*, 113406.
22. Auwärter, W.; Muntwiler, M.; Osterwalder, J.; Greber, T. Defect Lines and Two-Domain Structure of Hexagonal Boron Nitride Films on Ni(111). *Surf. Sci.* **2003**, *545*, L735–L740.
23. Müller, F.; Stöwe, K.; Sachdev, H. Symmetry *versus* Commensurability: Epitaxial Growth of Hexagonal Boron Nitride on Pt(111) from B-Trichloroborazine $(ClBNH)_3$. *Chem. Mater.* **2005**, *17*, 3464–3467.
24. Auwärter, W.; Suter, H.; Sachdev, H.; Greber, T. Synthesis of One Monolayer of Hexagonal Boron Nitride on Ni (111) from B-Trichloroborazine $(ClBNH)_3$. *Chem. Mater.* **2004**, *16*, 343–345.
25. Schulz, F.; Drost, R.; Hämäläinen, S. K.; Demonchaux, T.; Seitsonen, A. P.; Liljeroth, P. Epitaxial Hexagonal Boron Nitride on Ir(111): A Work Function Template. *Phys. Rev. B* **2014**, *89*, 235429.
26. Coraux, J.; N'Diaye, A. T.; Engler, M.; Busse, C.; Wall, D.; Buckanie, N.; zu Heringdorf, F.-J. M.; van Gastel, R.; Poelsema, B.; Michely, T. Growth of Graphene on Ir(111). *New J. Phys.* **2009**, *11*, 023006.
27. Usachov, D.; Fedorov, A.; Vilkov, O.; Adamchuk, V. K.; Yashina, L. V.; Bondarenko, L.; Saranin, A.; Grüneis, A.; Vyalikh, D. Experimental and Computational Insight into the Properties of the Lattice-Mismatched Structures: Monolayers of h-BN and Graphene on Ir(111). *Phys. Rev. B* **2012**, *86*, 155151.
28. Martoccia, D.; Brugger, T.; Björck, M.; Schlepütz, C.; Pauli, S.; Greber, T.; Patterson, B.; Willmott, P. *H*-BN/Ru (0001) Nanomesh: A 14-on-13 Superstructure with 3.5 nm Periodicity. *Surf. Sci.* **2010**, *604*, L16–L19.
29. Roth, S.; Matsui, F.; Greber, T.; Osterwalder, J. Chemical Vapor Deposition and Characterization of Aligned and Incommensurate Graphene/Hexagonal Boron Nitride Heterostack on Cu(111). *Nano Lett.* **2013**, *13*, 2668–2675.
30. Preobrajenski, A. B.; Nesterov, M. A.; Ng, M. L.; Vinogradov, A. S.; Mårtensson, N. Monolayer h-BN on Lattice-Mismatched Metal Surfaces: On the Formation of the Nanomesh. *Chem. Phys. Lett.* **2007**, *446*, 119–123.

31. García de Abajo, F. J.; Van Hove, M. A.; Fadley, C. S. Multiple Scattering of Electrons in Solids and Molecules: A Cluster-Model Approach. *Phys. Rev. B* **2001**, *63*, 075404.
32. Laskowski, R.; Blaha, P.; Schwarz, K. Bonding of Hexagonal BN to Transition Metal Surfaces: An *ab Initio* Density-Functional Theory Study. *Phys. Rev. B* **2008**, *78*, 045409.
33. Muntwiler, M.; Auwärter, W.; Baumberger, F.; Hoesch, M.; Greber, T.; Osterwalder, J. Determining Adsorbate Structures from Substrate Emission X-ray Photoelectron Diffraction. *Surf. Sci.* **2001**, *472*, 125–132.
34. Grad, G. B.; Blaha, P.; Schwarz, K.; Auwärter, W.; Greber, T. Density Functional Theory Investigation of the Geometric and Spintronic Structure of h-BN/Ni(111) in View of Photoemission and STM Experiments. *Phys. Rev. B* **2003**, *68*, 085404.
35. Laskowski, R.; Blaha, P.; Gallauner, T.; Schwarz, K. Single-Layer Model of the Hexagonal Boron Nitride Nanomesh on the Rh(111) Surface. *Phys. Rev. Lett.* **2007**, *98*, 106802.
36. Laskowski, R.; Blaha, P. *Ab Initio* Study of h-BN Nanomeshes on Ru(001), Rh(111), and Pt(111). *Phys. Rev. B* **2010**, *81*, 075418.
37. Lu, J.; Yeo, P. S. E.; Zheng, Y.; Xu, H.; Gan, C. K.; Sullivan, M. B.; Castro Neto, A. H.; Loh, K. P. Step Flow *versus* Mosaic Film Growth in Hexagonal Boron Nitride. *J. Am. Chem. Soc.* **2013**, *135*, 2368–2373.
38. Bianchi, M.; Cassese, D.; Cavallin, A.; Comin, R.; Orlando, F.; Postregna, L.; Golfetto, E.; Lizzit, S.; Baraldi, A. Surface Core Level Shifts of Clean and Oxygen Covered Ir(111). *New J. Phys.* **2009**, *11*, 063002.
39. Wideman, T.; Sneddon, L. G. Convenient Procedures for the Laboratory Preparation of Borazine. *Inorg. Chem.* **1995**, *34*, 1002–1003.
40. Doniach, S.; Šunjić, M. Many-Electron Singularity in X-ray Photoemission and X-ray Line Spectra from Metals. *J. Phys. C* **1970**, *3*, 285–291.
41. Lizzit, S.; Baraldi, A.; Grütter, C.; Bilgram, J.; Hofmann, P. The Surface Phase Transition and Low-Temperature Phase of α-Ga(010) Studied by SPA-LEED. *Surf. Sci.* **2009**, *603*, 3222–3226.
42. Locatelli, A.; Knox, K. R.; Cvetko, D.; Mentes, T. O.; Niño, M. A.; Wang, S.; Yilmaz, M. B.; Kim, P.; Osgood, R. M.; Morgante, A. Corrugation in Exfoliated Graphene: An Electron Microscopy and Diffraction Study. *ACS Nano* **2010**, *4*, 4879–4889.